International Journal of Nanomedicine

Dovepress
open access to scientific and medical research

Open Access Full Text Article

ORIGINAL RESEARCH

Multifunctional Graphene Oxide Nanodelivery Platform for Breast Cancer Treatment

Yousheng Mo[1,*], Wei Liu[2,*], Piaoxue Liu[2], Qiao Liu[3], Zhongyu Yuan[4], Qi Wang[2], Dongsheng Yuan[2], Xiao-Jia Chen[3], Tongkai Chen[2]

[1]The Second Affiliated Hospital of Guangzhou University of Chinese Medicine, Guangzhou, 510120, People's Republic of China; [2]Science and Technology Innovation Center, Guangzhou University of Chinese Medicine, Guangzhou, 510405, People's Republic of China; [3]State Key Laboratory of Quality Research in Chinese Medicine, Institute of Chinese Medical Sciences, University of Macau, Macau, 999078, People's Republic of China; [4]Department of Medical Oncology, Sun Yat-Sen University Cancer Center, the State Key Laboratory of Oncology in South China, Collaborative Innovation Center for Cancer Medicine, Guangzhou, 510060, People's Republic of China

*These authors contributed equally to this work

Correspondence: Xiao-Jia Chen; Tongkai Chen, Email xiaojiachen@um.edu.mo; chentongkai@gzucm.edu.cn

International Journal of Nanomedicine downloaded from https://www.dovepress.com/
For personal use only.

Background: Breast cancer (BC) has the highest global prevalence among all malignancies in women and the second highest prevalence in the overall population. Paclitaxel (PTX), a tricyclic diterpenoid, is effective against BC. However, its poor solubility in water and the allergenicity of its dissolution medium limited its clinical application.

Methods: In this work, we established a multifunctional graphene oxide (GO) tumor-targeting drug delivery system using nanosized graphene oxide (nGO) modified with D-tocopherol polyethylene glycol succinate (TPGS) and arginine-glycine-aspartic acid (RGD) for PTX loading.

Results: The obtained RGD-TPGS-nGO-PTX was 310.20±19.86 nm in size; the polydispersity index (PDI) and zeta potential were 0.21±0.020 and −23.42 mV, respectively. The mean drug loading capacity of RGD-TPGS-nGO-PTX was 48.78%. RGD-TPGS-nGO-PTX showed satisfactory biocompatibility and biosafety and had no significant toxic effects on zebrafish embryos. Importantly, it exerted excellent cytotoxicity against MDA-MB-231 cells, reversed multi-drug resistance (MDR) in MCF-7/ADR cells, and showed significant anti-tumor efficacy in tumor-bearing nude mice.

Conclusion: These findings strongly suggested that the multifunctional GO tumor-targeting drug delivery system RGD-TPGS-nGO-PTX could be used in clinical settings to improve PTX delivery, reverse MDR and increase the therapeutic efficacy of BC treatment.

Keywords: breast cancer, paclitaxel, targeted delivery, multidrug resistance

Introduction

Breast cancer (BC) has the highest global prevalence among all malignancies in women and the second highest prevalence in the overall population.[1] The most common therapeutic strategies for BC conservative surgery, radiation therapy, and chemotherapy cause several adverse effects, including lymphedema, damage to normal tissue, and tumor recurrence.[2–4] Pharmacological strategies are indispensable to accessible and effective treatments for BC patients.[5,6] Nevertheless, the drugs currently used to treat BC have unsatisfactory efficacy due to poor tumor targeting and drug resistance.[7,8] Therefore, new strategies must be explored for improving drug efficacy and targeting, overcoming drug resistance, and reducing off-target toxicity.

Nanomedicine has entered the field of view of researchers for its excellent targeted therapeutic properties. The known nanocarriers for targeted therapy of breast cancer include albumin-coated copper nanoparticles (ACuNPs),[9] chitosan/carbon quantum dot/aptamer complex (CS-CQD-apt),[10] agarose-polyethylene pyridoxanidone-hydroxyapatite (AG-PVP-Hap)[11] and many other nanocarriers. In addition, a variety of novel nanomaterials with excellent performance have been developed to significantly enhance the bioavailability, biocompatibility, and tumor targeting of natural compounds such as curcumin[12] and sesamol.[13,14]

Received: 29 June 2022
Accepted: 9 December 2022
Published: 15 December 2022

© 2022 Mo et al. This work is published and licensed by Dove Medical Press Limited. The full terms of this license are available at https://www.dovepress.com/terms.php and incorporate the Creative Commons Attribution – Non Commercial (unported, v3.0) License (http://creativecommons.org/licenses/by-nc/3.0/). By accessing the work you hereby accept the Terms. Non-commercial uses of the work are permitted without any further permission from Dove Medical Press Limited, provided the work is properly attributed. For permission for commercial use of this work, please see paragraphs 4.2 and 5 of our Terms (https://www.dovepress.com/terms.php).

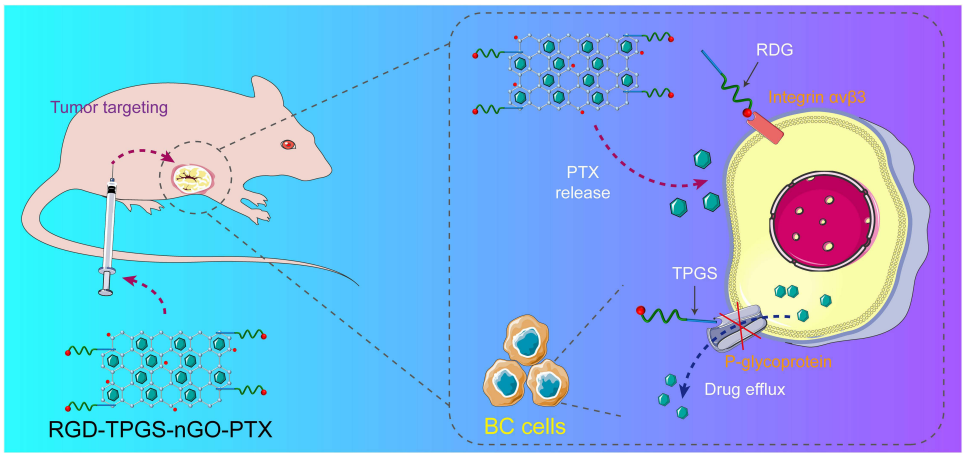

Scheme 1 Schematic of the in vitro and in vivo studies on the anti-tumor effects of RGD-TPGS-nGO-PTX.

Graphene oxide (GO), an oxidized form of graphene, has recently been developed as a novel two-dimensional carbon nanomaterial.[15] It has received extensive attention in drug delivery studies due to their good biocompatibility and low toxicity.[16,17] The surface of GO has hydrophilic groups, including hydroxyl (–OH), carboxyl (–COOH) and methoxyl (CH_3O-) groups, which can be modified and biofunctionalized.[18] Furthermore, nanosized GO (nGO) possesses good dispersity in water and also has a smaller particle size and good stability.[19] Importantly, nGO has a high drug loading capacity and excellent photothermal conversion performance and is easy to prepare.[20]

One major challenge in the efficient treatment of cancer is MDR.[21] In BC, MDR is often caused by an increase in P-glycoprotein (P-gp) expression on the surface of tumor cells.[22] As an ATP-powered efflux pump, P-gp removes anti-tumor drugs from cancer cells, rendering them ineffective.[23] D-tocopherol polyethylene glycol succinate (TPGS), which has received approval from the US Food and Drug Administration, is a multifunctional drug excipient with good biocompatibility.[24] TPGS has been reported to reverse MDR by inhibiting P-gp transport system,[25] and is also robust in prolonging the retention time of anti-tumor drug in cancer cells and enhancing the drug accumulation.[26]

Integrin αvβ3 is an important member of the integrin family. This protein has a series of functions in tumors, and is involved in angiogenesis, cell proliferation, invasion, and metastasis in different cancer types.[27,28] Integrin αvβ3 is closely associated with angiogenesis in BC.[29] Reports showed that arginine-glycine-aspartic acid (RGD) sequences specifically bind to integrin αvβ3.[30,31] Moreover, recent studies have confirmed that RGD can act as an excellent tumor-targeting ligand and that RGD-conjugated nano-carriers can target tumors effectively.[32]

Paclitaxel (PTX), a tricyclic diterpenoid present in bark and needles from the plant *Taxus brevifolia*, is used to treat several malignancies, including BC and ovarian, head and neck, and lung cancers.[33–36] However, PTX has many disadvantages, such as poor water solubility, poor tumor targeting, lack of efficacy in cases of multi-drug resistance (MDR), and low bioavailability, which limits its clinical application.[37–41] Recently, the research on the use of nanomaterials to solve these problems has gained wide attention.[42–44]

Given the specific properties of BC, such as MDR and the role of integrin αvβ3, as well as the drawbacks of PTX, we attempted to develop a system that allows targeted PTX delivery, reversal of MDR, and enhanced treatment efficacy against BC. Therefore, we established a multifunctional nGO tumor-targeting drug delivery system (RGD-TPGS-nGO-PTX). We first synthesized and characterized this system and then evaluated its anti-tumor effects in vitro as well as in vivo (Scheme 1).

Materials and Methods

Materials

PTX and GO were purchased from Nantong Feiyu Biological Technology Co., Ltd (Nantong, China) and Qingdao Baichuan Graphite Co., Ltd (Qingdao, China). TPGS was obtained from Shanghai YuanYe Biotechnology Co., Ltd (Shanghai, China). RGD was obtained from Qiangyao Biotechnology Co. Ltd. (Shanghai, China).

Dulbecco's Modified Eagle Medium (DMEM), Roswell Park Memorial Institute (RPMI) 1640 medium, fetal bovine serum (FBS), and penicillin-streptomycin were purchased from GIBCO, Invitrogen Corporation (USA). MTT solution was purchased from Sigma Aldrich (USA). The live/dead viability assay kit was obtained from Nanjing KeyGen Biotech. Inc. (Nanjing, China).

MDA-MB-231 human breast cancer cells and MCF-7/ADR cells were obtained from the Science and Technology Innovation Center of Guangzhou University of Chinese Medicine (Guangzhou, China) and Beijing Cell bank (Beijing, China), respectively. Zebrafish wild-type AB lines were purchased from China Zebrafish Resource Center (Wuhan, China). Female BALB/c-Nude mice (4–5 weeks of age) were purchased from SPF (Beijing) Biotechnology Co., Ltd. (Beijing, China).

All flasks and plates used for cell culture were obtained from Corning Costar Corp. (Cambridge, MA, USA). The Milli-Q Plus System (Millipore Corporation, Bedford, MA, USA) was used to obtain ultrapure water.

Synthesis of GO and nGO

GO was prepared using a modified version of Hummer's method. Briefly, 4 g of graphite powder was added to 100 mL of H_2SO_4 kept on ice, and the mixture was stirred continuously. Subsequently, 25 g $KMnO_4$ was added slowly, and the mixture was incubated at a constant temperature of 35°C for 1 h. Further, 200 mL of deionized water was added to the reaction mixture, and the mixture was incubated at 98°C for 30 min. Subsequently, the mixture underwent filtration and thorough washes with deionized water until a pH of 7 was reached. The mixture was then dried under vacuum at 60°C, and GO was obtained. The GO was then suspended in deionized water and broken into small particles using an ultrasonic cell crusher, and nGO was obtained after filtration and freeze-drying (Figure 1A).

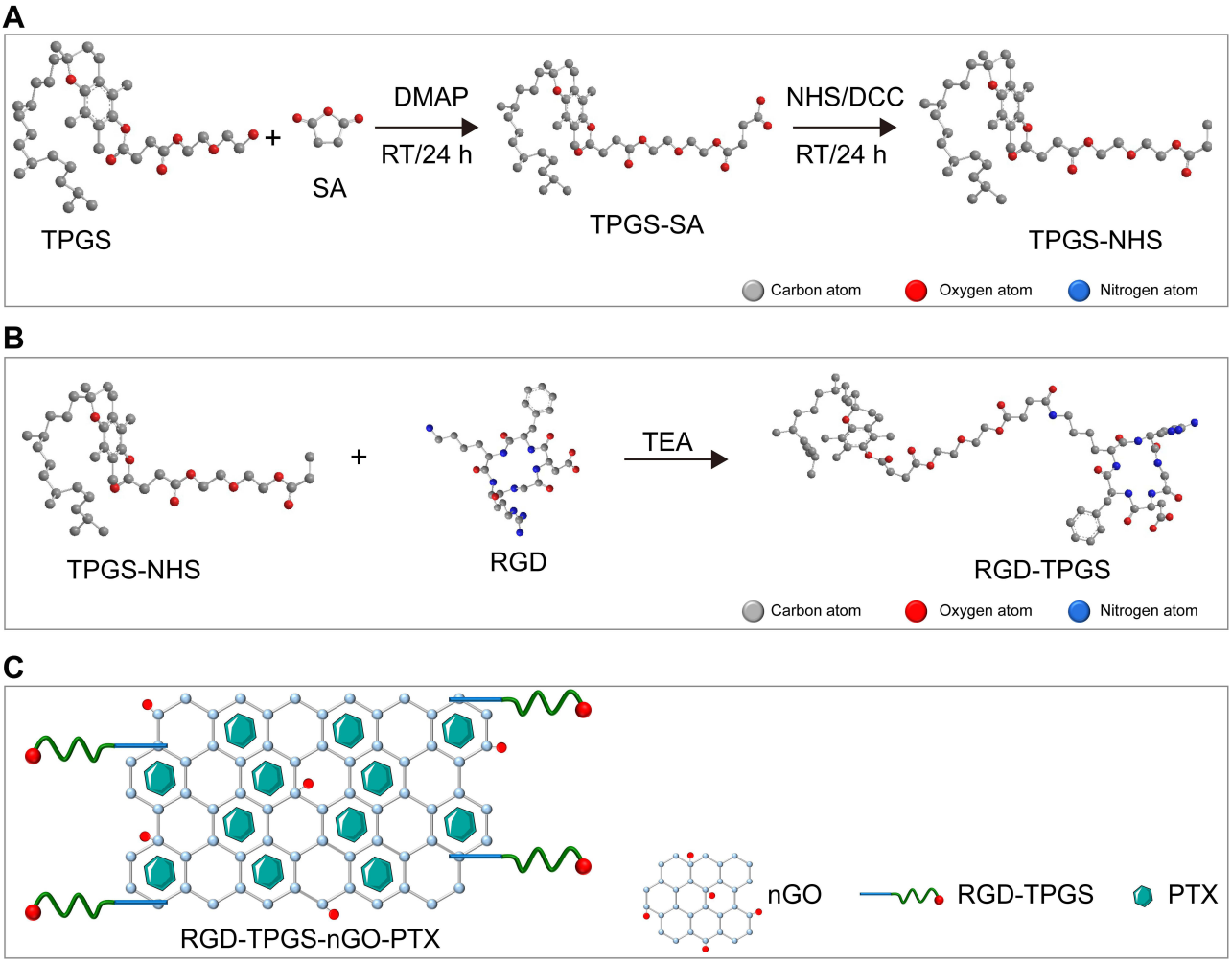

Figure 1 Schematic of RGD-TPGS-nGO-PTX synthesis. Synthesis of TPGS-NHS (**A**), RGD-TPGS (**B**), and RGD-TPGS-nGO-PTX (**C**).

Synthesis of TPGS-RGD: TPGS-RGD was prepared as described in the previous study.[24] In brief, TPGS, succinic anhydride (SA), and 4-dimethylaminopyridine (DMAP) were dissolved in 15 mL of dichloromethane. The mixture was stirred constantly for 24 h and then underwent filtration and dialysis. The resultant TPGS-SA was stored at 4°C. Next, TPGS-SA, N-hydroxysuccinimide (NHS), and N, N'-dicyclohexylcarbodiimide (DCC) were dissolved in 10 mL of dichloromethane; the mixture was stirred and then filtered to obtain the intermediate product TPGS-NHS. Following this, TPGS-NHS and RGD were dissolved in dimethylformamide (DMF). The mixture was stirred constantly for 24 h and triethylamine was added in a dropwise manner. The resultant TPGS-RGD was obtained after filtration and dialysis (Figure 1B).

Synthesis of RGD-TPGS-nGO-PTX: RGD-TPGS-nGO-PTX was prepared as previously described.[17] A 1 mL nGO solution was mixed with 1 mL of a PTX solution at room temperature for 24 h under constant stirring to allow PTX to adsorb onto nGO. Next, nGO-PTX was mixed with TPGS-RGD at the ratio of 1:1 followed by dialysis and vacuum freeze drying to obtain RGD-TPGS-nGO-PTX (Figure 1C).

RGD-TPGS-nGO-PTX Characterization

nGO, RGD-TPGS-nGO, and RGD-TPGS-nGO-PTX were characterized. The morphology of these particles was observed using a transmission electron microscope (TEM) (H-600, Hitachi, Japan), and the particle size and zeta potential analysis were using Dynamic Light Scattering (DLS) (NICOMP 380 Z3000, US). We examined the intermediate products and the functional groups of particles using FT-IR (Nicolet™ iN10 MX Infrared Imaging Microscope/ Nicolet 6700 FT-IR Spectrometer). Elemental analysis was performed using a Vario EL cube (Elementar). To detect the drug-loading capacity of RGD-TPGS-nGO-PTX, we created standard curves of absorbance vs concentration for PTX. External calibration was used to determine drug loading. To determine stability, RGD-TPGS-nGO, nGO, and RGD-TPGS-nGO were diluted to 0.25 mg/mL in 0.9% saline or double-distilled water. The diluted samples were placed on the stage of a tester and stability was observed on the first, third, seventh, and fifteenth days.

Cell Culture and Animal Care

The study received approval from the Animal Ethics Committee of Guangzhou University of Chinese Medicine and followed all national regulations for the care and use of experimental animals.

We cultured MDA-MB-231 cells (human breast cancer cells) in DMEM (containing 10% FBS and 100 U/mL of penicillin and streptomycin each) under sterile conditions at 37°C and 5% CO_2. In contrast, we cultured MCF-7/ADR cells (human breast carcinoma cells showing drug resistance) in RPMI 1640 medium (containing 10% heat-inactivated FBS, 100 U/mL penicillin G, and 100 μg streptomycin) at 37°C and 5% CO_2.

Wild-type zebrafish were grown under a 14/10 h light/dark cycle at 28.0±1°C (pH, 6.8–7.5). At maturity, male and female zebrafish were added to a fertilization tank at a 1:1 ratio. Following the light cycle, fertilized embryos were collected, and 1-phenyl-2-thiourea treatment was used to prevent pigment development.

BALB/c-nu/nu female mice (4–5 weeks old) were maintained under 12 h light/dark cycles at 23±2°C and 50±20% relative humidity. They all received standard laboratory chow and water ad libitum.

In vivo Examination of Toxicity

Zebrafish are widely used in drug discovery, drug development, and toxicological screening as a small vertebrate model,[45,46] owing to the high similarity between their morphology and physiology and that of mammals[39,45] Moreover, zebrafish embryos and larvae are almost transparent, which enables the easy surveillance of organ development.[47,48] In this study, healthy zebrafish embryos (5 hpf) were placed in 24-well dishes (20 per well) and treated with 250 μg/mL of nGO, TPGS, and RGD-TPGS-nGO. The survival rate of zebrafish embryos was evaluated based on their heartbeat, activity, and circulation at 96 hpf. The hatching rate, heart rate, and body length were also examined at this stage.

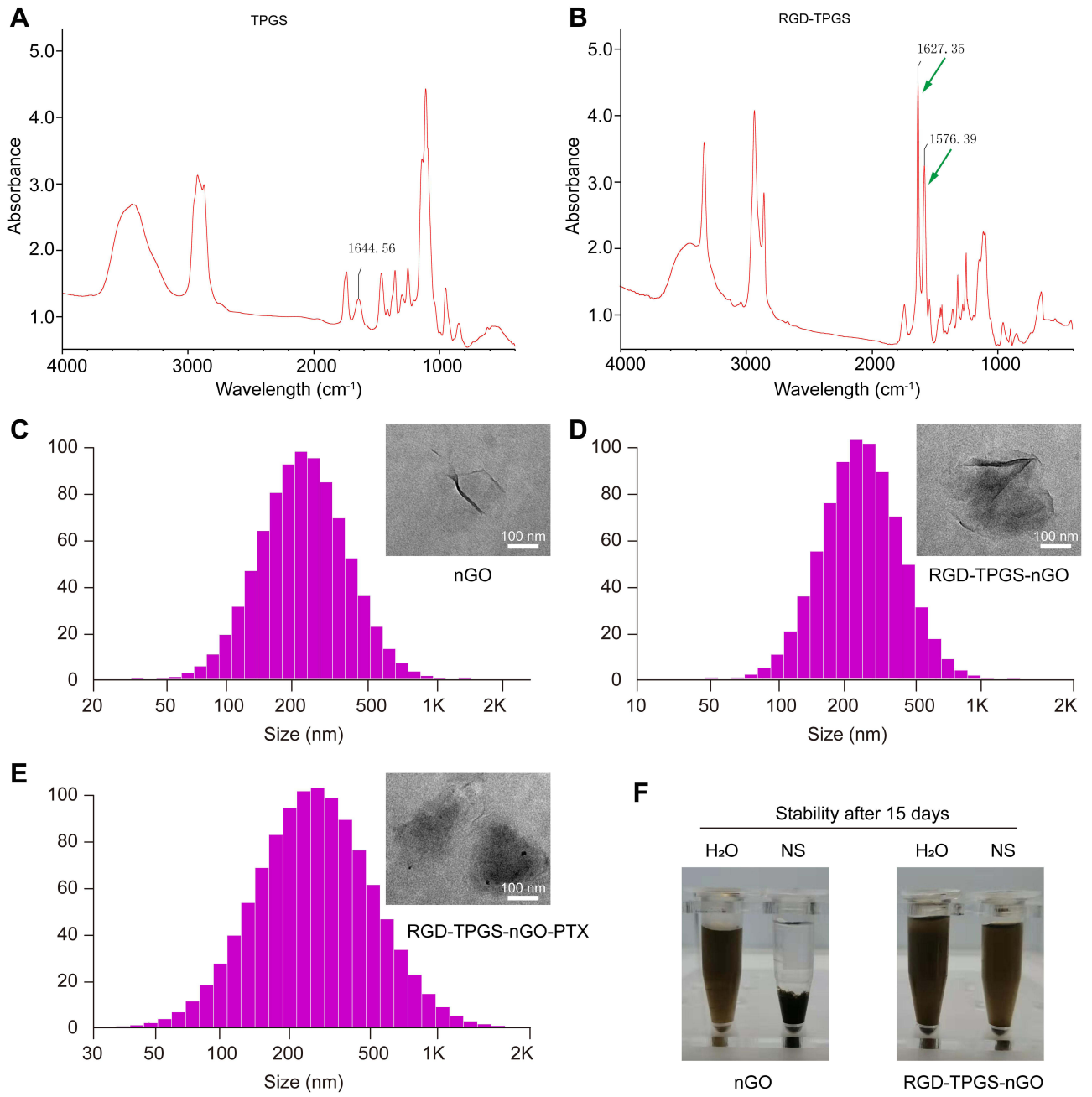

Figure 2 Characterization of RGD-TPGS-nGO-PTX. FT-IR analysis spectroscopy of TPGS (**A**) and RGD-TPGS (**B**), green arrows indicate which are the unique infrared peaks of the amide bond. Representative corresponding particle size parameters and TEM images (right) (**C**–**E**). (**F**) Stability analysis of nGO and GD-TPGS-nGO, the samples were dispersed in double-distilled water (H_2O) or 0.9% normal saline (NS) at a concentration of 0.25 mg/mL.

Cell Viability Assay

The viability of MCF-7/ADR cells was examined with MTT assays. After 24 h of culture, cells were treated with different concentrations of RGD-TPGS-nGO-PTX. The supernatant was discarded after 24 h of incubation, and 90 μL DMEM and 10 μL MTT solution was added to each well; the cells were then incubated in the dark for 4 h. Following this, 150 μL dimethyl sulfoxide (DMSO) (Guangzhou Chemical Reagent Factory, Guangzhou, China) was added to each well after discarding the supernatant, and cells were incubated for 10 min with shaking. A microplate reader (Multiskan FC, Thermo Scientific, United States) was used to measure absorbance at 490 nm and cell viability was calculated.

Live/Dead Cell Staining

MDA-MB-231 cells were seeded in culture medium (5×10^4 cells per well) and allowed to attach. After 24 h, the old medium was discarded and fresh medium containing RGD-TPGS-nGO, PTX, or RGD-TPGS-nGO-PTX was added. The cells were treated with different concentration of the agents (1.25, 0.625, 0.3125, 0.15625 μg/mL) for 24 h. Subsequently, the supernatant was discarded, and the cells were incubated in the staining solution (2 μM calcein-AM and 8 μM PI) for 30 min under dark conditions. Finally, the cells were imaged using a fluorescence microscope (DMi8, Leica, Germany).

Mitochondrial Oxygen Consumption

MCF-7/ADR cells were seeded in culture medium (3×10^3 cells per well) and allowed to attach for 24 h. After the cells were treated with different agents, OCR was examined using a Seahorse XF96 Extracellular Flux analyzer (Seahorse Bioscience, MA, USA).

For another set of experiments, the MCF-7/ADR cells were cultured in medium (2.5×10^4 cells per well) for 24 h and subsequently treated with nG, TPGS-nGO, and RGD-TPGS-nGO (25, 50, and 100 μM), and 10 μM NaN3 solution was used as the positive control group. After 36 h of incubation, the old media were replaced with 175 μL of FX Assay-Modified DMEM containing 5.5 mM glucose, 1 mM pyruvate, and 2 mM glutamine (Agilent Technologies) and cells were cultured in a CO_2-free incubator for 1 h. Mitochondrial and cellular metabolic profiles were then obtained using a mitochondrial stress assay.[49]

Animal Groups and Treatment

We injected a 200 μL suspension of MDA-MB-231 cells (1.12×10^7 cells/mL) into the mammary fat pad of 20 female BALB/c-Nude mice to establish an orthotopic mouse model of BC. When tumors grew to 40–60 mm^3 in volume, the mice were randomized into the control, PTX, TPGS-nGO-PTX, and RGD-TPGS-nGO-PTX groups (n = 5/group). Mice in the PTX, TPGS-nGO-PTX and RGD-TPGS-nGO-PTX groups received i.p. injections of 5 mg/kg PTX, TPGS-nGO-PTX, and RGD-TPGS-nGO-PTX, once every three days for 30 days. Equal volumes of normal saline were administered to the control group via i.p. injections over the same time points.

Assessment of Anti-Tumor Effect and PTX Content in Tumors

After the final drug treatment, mice were weighed and euthanized. Tumor tissue samples (100 mg) were collected from each group and homogenized in 70% methanol. Homogenates underwent centrifugation at 12,000 ×g at 4°C for 10 min. Subsequently, PTX concentrations in the tumor tissues of mice from each group were detected by analyzing the collected supernatant with high-performance liquid chromatography.

Table 1 The Characteristic Parameters Include Particle Size, PDI and Zeta Potential

	Particle Size (nm)	PDI	Zeta Potential (mV)
nGO	266.63±9.59	0.21±0.03	−30.2
RGD-TPGS-nGO	312.23±13.17	0.29±0.05	−26.42
RGD-TPGS-nGO-PTX	310.20±19.86	0.21±0.02	−23.42

Note: Data are presented as mean ± standard deviation, N=3.

Table 2 Organic Element Analysis

	nGO	TPGS-nGO	RGD-TPGS-nGO
N [%]	0	0	3.36±0.28
C [%]	44.92±0.96	55.24±0.27	53.98±0.47
H [%]	2.30±0.17	6.63±0.05	8.00±0.14

Note: Data are presented as mean ± standard deviation, N=3.

Statistical Analysis

All the data are expressed as means ± standard deviations. All multiple-group comparisons were performed using one-way analysis of variance, and differences between two groups were analyzed using two-tailed Student's *t*-tests. A *P*-value less than 0.05 was considered to indicate statistical significance.

Results and Discussion

Characterization of the Synthesized TPGS-RGD

To better verify the accuracy of synthesis, we performed FTIR detection of TPGS and TPGS-RGD. According to Figure 2A and B, the functional group types of TPGS and TPGS-RGD are basically similar. In the infrared spectrum of TPGS-RGD, compared with TPGS, there are two characteristic absorption peaks at 1576.39 cm^{-1} and 1627.35 cm^{-1}, which are the unique infrared absorption peaks of the amide bond. It is proved that TPGS and RGD can combine smoothly through an amide bond to produce a new compound TPGS-RGD.

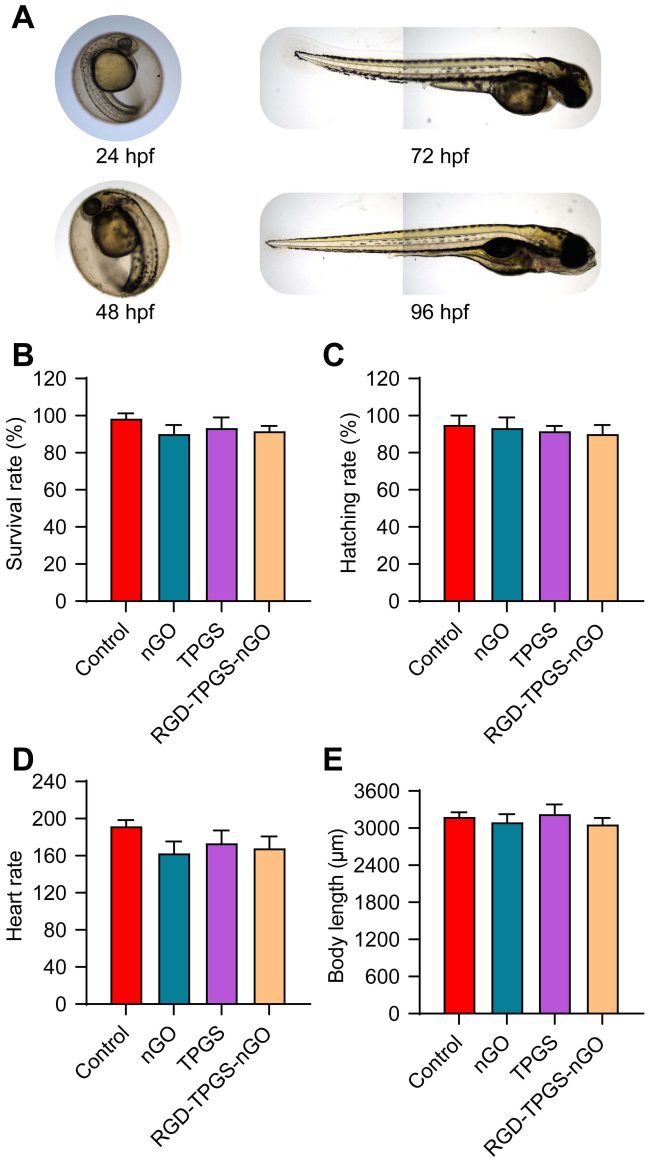

Figure 3 Assessment of RGD-TPGS-nGO toxicity in vivo. (**A**) Morphological characterization, (**B**) Survival rate, (**C**) hatching rate, (**D**) heart rate, and (**E**) body length of zebrafish at 96 hours post-fertilization (hpf). Data are presented as mean ± standard deviation. The error bars represent the standard deviation values of ten independent repeats.

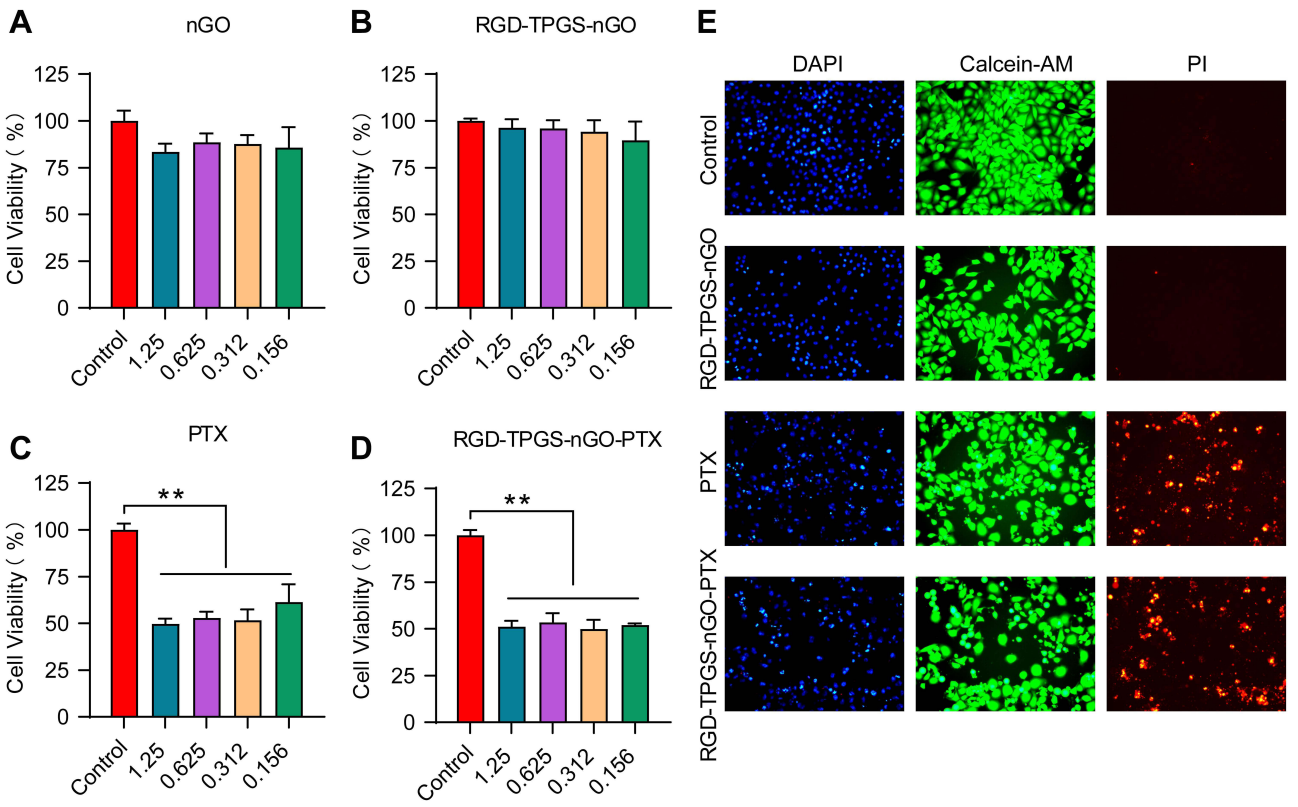

Figure 4 Assessment of the in vitro anti-tumor effect of RGD-TPGS-nGO-PTX. The survival rate of MDA-MB-231 cells after nGO (**A**), RGD-TPGS-nGO (**B**), PTX (**C**), and RGD-TPGS-nGO-PTX (**D**) administration. (**E**) Live/dead cell staining of MDA-MB-231 cells after treatment with different agents. Live cells were stained with Calcein-AM and dead cells were stained with PI. Data are presented as mean ± standard deviation. The error bars represent the standard deviation values of six independent repeats. $^{**}p<0.01$.

Characterization of RGD-TPGS-nGO-PTX

DLS graph shows that nGO, RGD-TPGS-nGO, and RGD-TPGS-NGO-PTX have roughly the same diameter (around 280nm). TEM results confirm the information obtained from DLS and show that the synthesized nanoparticles are roughly irregular in shape with clear edges (Figure 2C–E). The PDI data show that these nanoparticles have good homogeneity. The zeta potential indicates the degree of electrostatic repulsion between adjacent nanoparticles, which is an important indicator of particle stability in solution. Studies have shown that particles with charges from ±10 to ±30 are generally considered to be stable.[9,11] Our data show that the synthesized RGD-TPGS-nGO-PTX has a suitable zeta potential (−23.42 mV), which indicates that it has good stability to a certain extent. The detailed characterization parameters are shown in Table 1.

In addition, we also performed a stability evaluation. In an aqueous medium, nGO and RGD-TPGS-nGO remained stable without any flocculation for 15 consecutive days. Although nGO showed visible precipitation and flocculation in saline on day 1 itself, RGD-TPGS-nGO showed excellent stability (Figure 2F). These findings indicated that the presence of RGD-TPGS may be suppressed the flocculation of nGO by masking the charged groups on the nGO surface. Additionally, TPGS acts as a surfactant and has dissolution-enhancing properties.[50] TPGS modification increased the viscosity of the nGO solution, leading to an inhibition of nanoparticle aggregation.[51]

The mean drug loading capacity of RGD-TPGS-nGO-PTX was 48.78%. Elemental analysis revealed that the elemental content of N in nGO, TPGS-nGO, and RGD-TPGS-nGO was 0%, 0%, and 3.36%, respectively, indicating that RGD-TPGS-nGO had RGD-containing peptides.[52] Further, the elemental content of H in these nanoparticles was 2.30%, 6.63%, and 8.00%, respectively, showing a clear increasing trend (Table 2).

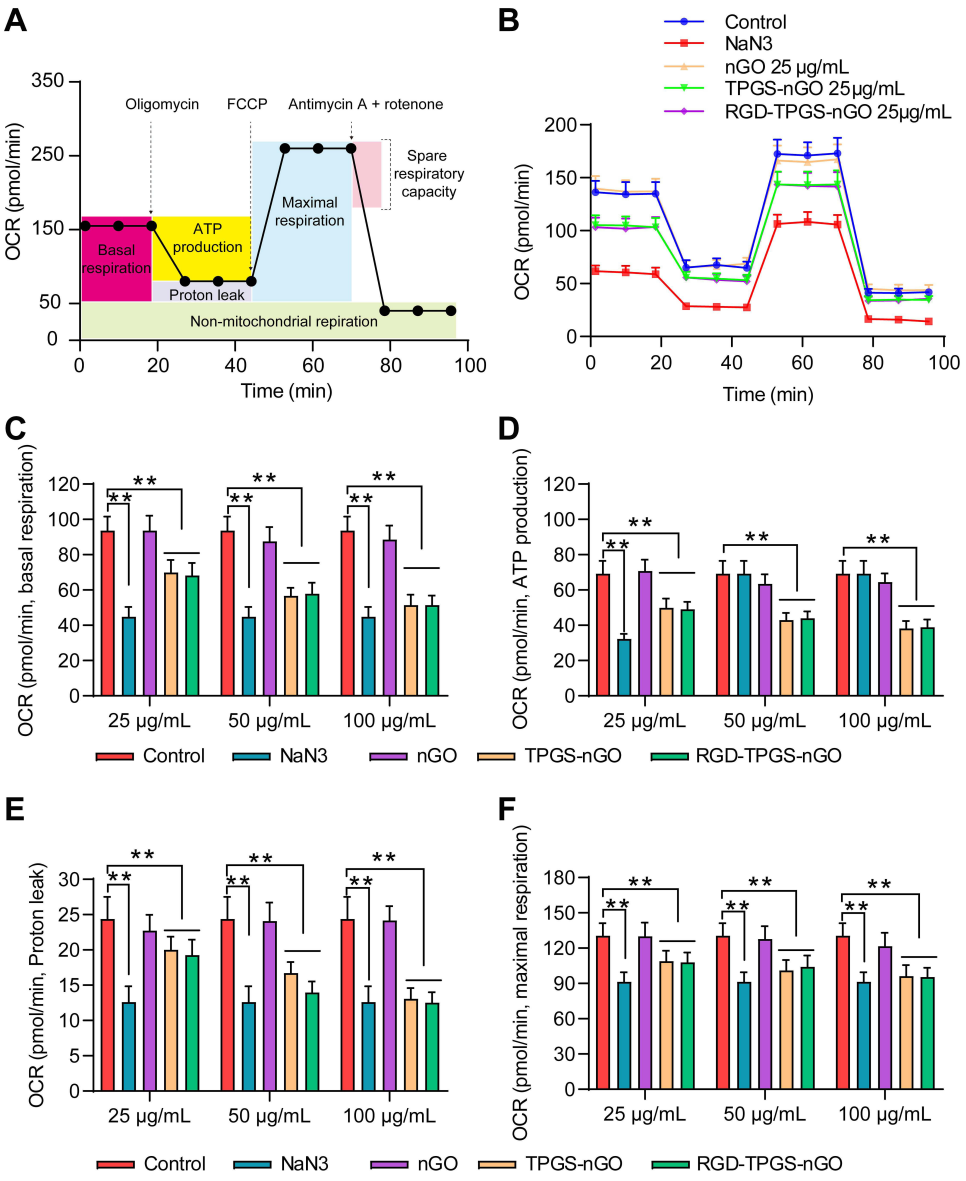

Figure 5 Effect of RGD-TPGS-nGO on OCR in MCF-7/ADR cells. (**A**) Schematic of OCR analysis. (**B**) Effect of 25 μg/mL concentrations of different agents on OCR in MCF-7/ADR cells. Effect of various concentrations of different agents on basal respiration (**C**), ATP production (**D**), proton leak (**E**), and maximal respiration (**F**) in mitochondria from MCF-7/ADR cells. Data are presented as mean ± standard deviation. The error bars represent the standard deviation values of five independent repeats. $^{**}p<0.01$.

Assessment of RGD-TPGS-nGO Toxicity

Zebrafish embryos are ideal models for testing drug toxicity in vivo because their optical transparency enables the monitoring of morphological changes (Figure 3A).[53,54] After incubation with 250 μg/mL of nGO, TPGS, and RGD-TPGS-nGO, zebrafish embryos were examined at 96 hours post-fertilization (hpf). The treated zebrafish embryos showed no significant differences in survival rate (Figure 3B), hatching rate (Figure 3C), heart rate (Figure 3D), and body length (Figure 3E) when compared with the control embryos. These results revealed that RGD-TPGS-nGO administration had no significant toxic effects on zebrafish embryos.

Assessment of the Anti-Tumor Effect of RGD-TPGS-nGO-PTX in vitro

We performed a 3-(4, 5-dimethylthiazol-2-yl)-2, 5-diphenyltetrazolium bromide (MTT) assay to assess the anti-tumor effect of RGD-TPGS-nGO-PTX in MDA-MB-231 cells. Treatment with GO and RGD-TPGS-nGO had no significant

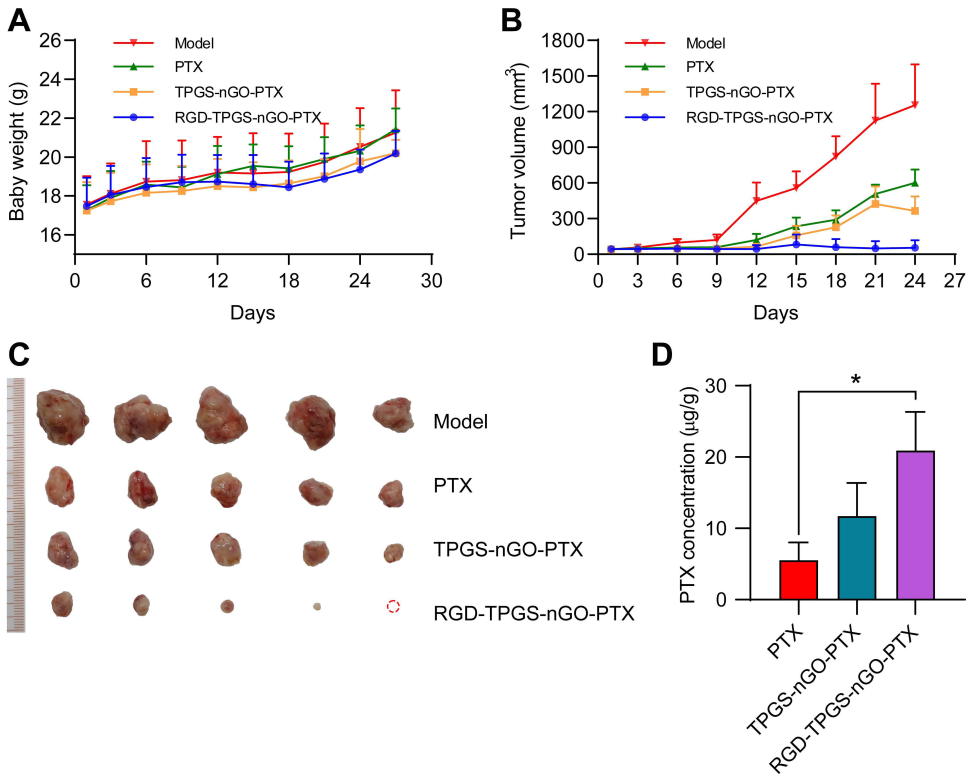

Figure 6 Assessment of the in vivo anti-tumor effect of RGD-TPGS-nGO-PTX. (**A**) Effect of RGD-TPGS-nGO-PTX on body weight in mouse models of breast cancer. (**B**) Effect of RGD-TPGS-nGO-PTX on tumor volume. Data are presented as mean ± standard deviation. Data are presented as mean ± standard deviation. The error bars represent the standard deviation values of five independent repeats. *p<0.05. (**C**) Representative images of tumor tissues from different groups of mice. (**D**) PTX concentrations in tumor tissues in the mice. Data are presented as mean ± standard deviation. The error bars represent the standard deviation values of three independent repeats. *p<0.05.

impact on cell survival (Figure 4A and B). However, PTX and RGD-TPGS-nGO-PTX effectively decreased tumor cell viability (Figure 4C and D). Moreover, live/dead cell staining revealed that while RGD-TPGS-nGO administration did not affect MDA-MB-231 cells, PTX and RGD-TPGS-nGO-PTX treatment caused a significant reduction in tumor cell survival (Figure 4E).

MDR Reversal by RGD-TPGS-nGO via Reductions in Mitochondrial Oxygen Consumption Rates

Mitochondria are the powerhouses of cells and are involved in several metabolic processes and conditions.[55,56] Mitochondrial respiratory function is associated with tumor occurrence, development, and MDR.[57,58] To further explore how RGD-TPGS-nGO treatment suppresses tumor cell survival and growth, we detected the mitochondrial oxygen consumption rate (OCR) in MCF-7/ADR cells (human breast carcinoma cells showing drug resistance) using an XF96 Extracellular Flux Analyzer (Figure 5A). Comparisons with the control, results showed that nGO treatment had no significant effect on mitochondrial basal respiration, ATP production, proton leak, and maximal respiration in MCF-7/ADR cells. However, different concentrations of TPGS-nGO and RGD-TPGS-nGO significantly inhibited these processes and impaired respiratory function in mitochondria (Figure 5B–F). Taken together, these findings indicated that RGD-TPGS-nGO treatment could reverse MDR in MCF-7/ADR cells by suppressing mitochondrial respiratory function.

Assessment of the Anti-Tumor Effect of RGD-TPGS-nGO-PTX in vivo

Animals in each group showed a significant increase in body weight over time, and these values were similar across all groups (Figure 6A). Furthermore, comparisons with the PTX and TPGS-nGO-PTX groups revealed that RGD-TPGS-nGO-PTX treatment attenuated the increase in tumor volume in mice (Figure 6B and C). Importantly, the RGD-TPGS-nGO-PTX

group showed significantly higher PTX content in tumor tissues than the PTX and TPGS-nGO-PTX groups (Figure 6D). These results suggested that RGD-modified nGO had significant tumor-targeting capabilities. Moreover, these findings strongly indicated that TPGS-modified nGO might increase the in vivo circulation time of PTX and reverse MDR in tumor cells. Finally, the increased deposition of PTX in tumors by RGD-TPGS-nGO could also improve the treatment response.

Conclusions

In this work, we established a multifunctional GO tumor-targeting drug delivery system using nGO modified with TPGS and RGD and loaded with PTX. RGD-TPGS-nGO administration showed no significant toxic effects in zebrafish embryos in vivo. Moreover, it could effectively suppress the survival of MDA-MB-231 cells and inhibit mitochondrial respiratory function in MCF-7/ADR cells in vitro. Further in vivo analyses in tumor-bearing mice showed that RGD-TPGS-nGO-PTX treatment significantly inhibits increases in tumor volume and enhances PTX concentrations in tumor tissue. These findings suggest that the RGD-TPGS-nGO nano delivery platform potential for enhancing PTX delivery and treatment efficacy in cases of BC.

Data Sharing Statement

The data that support the findings of this study are available from the corresponding author (Tongkai Chen) upon reasonable request.

Acknowledgments

This work was supported by the Key laboratory project of colleges and universities in Guangdong province (2019KSYS005), the Guangdong province science and technology plan international cooperation project (2020A0505100052), the Guangdong Basic and Applied Basic Research Foundation (2019B1515120043), the Research Fund of University of Macau (File no. MYRG2019-00121-ICMS and MYRG2018-00207-ICMS), the Science and Technology Development Fund, Macau SAR (File no. 0098/2020/A), the Key Sci-Tech Research Project of Guangzhou Municipality (202002020033), the Key Project of Basic Research of Shenzhen (JCYJ20200109113603854) and the Guangdong Provincial Natural Science Foundation of China (2018A030310623).

Disclosure

The authors declare no potential conflicts of interest with respect to the authorship and/or publication of this article.

References

1. Kotsopoulos J. Menopausal hormones: definitive evidence for breast cancer. *Lancet*. 2019;394:1116–1118. doi:10.1016/S0140-6736(19)31901-4
2. McClelland S. Breast cancer radiation therapy. *Lancet*. 2020;396:1559. doi:10.1016/S0140-6736(20)32324-2
3. Prat A, Guarneri V, Pare L, et al. A multivariable prognostic score to guide systemic therapy in early-stage HER2-positive breast cancer: a retrospective study with an external evaluation. *Lancet Oncol*. 2020;21:1455–1464. doi:10.1016/S1470-2045(20)30450-2
4. Shieh Y, Tice JA. Medications for primary prevention of breast cancer. *JAMA*. 2020;324:291–292. doi:10.1001/jama.2020.9246
5. Onishi S, Sawaki M, Ishiguro J, et al. The overall survival of breast cancer patients without adjuvant therapy. *Surg Today*. 2019;49:610–620. doi:10.1007/s00595-019-01775-z
6. Shimomura A, Yonemori K, Yoshida M, et al. Gene alterations in triple-negative breast cancer patients in a phase I/II study of eribulin and olaparib combination therapy. *Transl Oncol*. 2019;12:1386–1394. doi:10.1016/j.tranon.2019.07.013
7. Curigliano G, Pravettoni G. Use of chemotherapy in elderly patients with early-stage triple-negative breast cancer comment. *Lancet Oncol*. 2020;21:1543–1545. doi:10.1016/S1470-2045(20)30694-X
8. Voelker R. Breast cancer drug can be given at home or in the clinic. *JAMA*. 2020;324:433.
9. Azizi M, Ghourchian H, Yazdian F, Dashtestani F, AlizadehZeinabad H. Cytotoxic effect of albumin coated copper nanoparticle on human breast cancer cells of MDA-MB 231. *PLoS One*. 2017;12. doi:10.1371/journal.pone.0188639
10. Zavareh HS, Pourmadadi M, Moradi A, Yazdian F, Omidi M. Chitosan/carbon quantumdot/aptamer complex as a potential anticancer drug delivery system towards the release of 5-fluorouracil. *Int J Biol Macromol*. 2020;165:1422–1430. doi:10.1016/j.ijbiomac.2020.09.166
11. Samadi A, Pourmadadi M, Yazdian F, Rashedi H, Navaei-Nigjeh M, Eufrasio-da-silva T. Ameliorating quercetin constraints in cancer therapy with pH-responsive agarose-polyvinylpyrrolidone -hydroxyapatite nanocomposite encapsulated in double nanoemulsion. *Int J Biol Macromol*. 2021;182:11–25. doi:10.1016/j.ijbiomac.2021.03.146
12. Abtahi NA, Naghib SM, Haghiralsadat F, et al. Smart stimuli-responsive biofunctionalized niosomal nanocarriers for programmed release of bioactive compounds into cancer cells in vitro and in vivo. *Nanotechnol Rev*. 2021;10:1895–1911. doi:10.1515/ntrev-2021-0119

13. Abdelhamid HN, El-Bery HM, Metwally AA, Elshazly M, Hathout RM. Synthesis of CdS-modified chitosan quantum dots for the drug delivery of Sesamol. *Carbohyd Polym*. 2019;214:90–99. doi:10.1016/j.carbpol.2019.03.024
14. ElMasry SR, Hathout RM, Abdel-Halim M, Mansour S. In Vitro transdermal delivery of sesamol using oleic acid chemically-modified gelatin nanoparticles as a potential breast cancer medication. *J Drug Deliv Sci Tec*. 2018;48:30–39. doi:10.1016/j.jddst.2018.08.017
15. Yan YX, Manickam S, Lester E, Wu T, Pang CH. Synthesis of graphene oxide and graphene quantum dots from miscanthus via ultrasound-assisted mechano-chemical cracking method. *Ultrason Sonochem*. 2021;73:105519. doi:10.1016/j.ultsonch.2021.105519
16. Maity AR, Chakraborty A, Mondal A, Jana NR. Carbohydrate coated, folate functionalized colloidal graphene as a nanocarrier for both hydrophobic and hydrophilic drugs. *Nanoscale*. 2014;6:2752–2758. doi:10.1039/c3nr05431d
17. Xu ZY, Wang S, Li YJ, Wang MW, Shi P, Huang XY. Covalent functionalization of graphene oxide with biocompatible poly(ethylene glycol) for delivery of paclitaxel. *Acs Appl Mater Inter*. 2014;6:17268–17276. doi:10.1021/am505308f
18. Orecchioni M, Cabizza R, Bianco A, Delogu LG. Graphene as cancer theranostic tool: progress and future challenges. *Theranostics*. 2015;5:710–723. doi:10.7150/thno.11387
19. Kurapati R, Russier J, Squillaci MA, et al. Dispersibility-dependent biodegradation of graphene oxide by myeloperoxidase. *Small*. 2015;11:3985–3994. doi:10.1002/smll.201500038
20. Song MM, Xu HL, Liang JX, Xiang HH, Liu R, Shen YX. Lactoferrin modified graphene oxide iron oxide nanocomposite for glioma-targeted drug delivery. *Mat Sci Eng C*. 2017;77:904–911. doi:10.1016/j.msec.2017.03.309
21. Li YP, Li R, Liu QH, et al. One-step self-assembling nanomicelles for pirarubicin delivery to overcome multidrug resistance in breast cancer. *Mol Pharmaceut*. 2016;13:3934–3944. doi:10.1021/acs.molpharmaceut.6b00712
22. van Vliet EA, Iyer AM, Mesarosova L, et al. Expression and cellular distribution of P-glycoprotein and breast cancer resistance protein in amyotrophic lateral sclerosis patients. *J Neuropath Exp Neur*. 2020;79:266–276. doi:10.1093/jnen/nlz142
23. Wang J, Gan CP, Retmana IA, et al. P-glycoprotein (MDR1/ABCB1) and Breast Cancer Resistance Protein (BCRP/ABCG2) limit brain accumulation of the FLT3 inhibitor quizartinib in mice. *Int J Pharmaceut*. 2019;556:172–180. doi:10.1016/j.ijpharm.2018.12.014
24. Chen YZ, Feng S, Liu WC, Yuan ZT, Yin PH, Gao F. Vitamin E succinate-grafted-chitosan oligosaccharide/RGD-conjugated TPGS mixed micelles loaded with paclitaxel for U87MG tumor therapy. *Mol Pharmaceut*. 2017;14:1190–1203. doi:10.1021/acs.molpharmaceut.6b01068
25. Tan X, Fang Y, Ren YY, et al. D-alpha-tocopherol polyethylene glycol 1000 succinate-modified liposomes with an siRNA Corona confer enhanced cellular uptake and targeted delivery of doxorubicin via tumor priming. *Int J Nanomed*. 2019;14:1255–1268. doi:10.2147/IJN.S191858
26. de Melo-Diogo D, Pais-Silva C, Costa EC, Louro RO, Correia IJ. D-alpha-tocopheryl polyethylene glycol 1000 succinate functionalized nanographene oxide for cancer therapy. *Nanomedicine-Uk*. 2017;12:443–456. doi:10.2217/nnm-2016-0384
27. Coskun MD, Sudha T, Bharali DJ, Celikler S, Davis PJ, Mousa S. A. alpha v beta 3 integrin antagonists enhance chemotherapy response in an orthotopic pancreatic cancer model. *Front Pharmacol*. 2020;11:115.
28. Ho Y, Li ZL, Shih YJ, et al. Integrin alpha v beta 3 in the mediating effects of dihydrotestosterone and resveratrol on breast cancer cell proliferation. *Int J Mol Sci*. 2020;21:2906. doi:10.3390/ijms21082906
29. Zhang JJ, Mao F, Niu G, et al. Ga-68-BBN-RGD PET/CT for GRPR and integrin alpha(v)beta(3) imaging in patients with breast cancer. *Theranostics*. 2018;8:1121–1130. doi:10.7150/thno.22601
30. Vatsa R, Bhusari P, Kumar S, et al. Integrin alpha(v)beta(3) as a promising target to image neoangiogenesis using in-house generator-produced positron emitter Ga-68-labeled DOTA-arginine-glycine-aspartic acid (RGD) ligand. *Cancer Biother Radio*. 2015;30:217–224.
31. Xiao WW, Wang Y, Lau EY, et al. The use of one-bead one-compound combinatorial library technology to discover high-affinity alpha v beta 3 integrin and cancer targeting arginine-glycine-aspartic acid ligands with a built-in handle. *Mol Cancer Ther*. 2010;9:2714–2723. doi:10.1158/1535-7163.MCT-10-0308
32. Fu S, Zhao YA, Sun J, et al. Integrin alpha v beta 3-targeted liposomal drug delivery system for enhanced lung cancer therapy. *Colloid Surface B*. 2021;201:111623. doi:10.1016/j.colsurfb.2021.111623
33. Dan VM, Raveendran RS, Baby S. Resistance to intervention: paclitaxel in breast cancer. *Mini Rev Med Chem*. 2021;21:1237–1268. doi:10.2174/1389557520999201214234421
34. Logue SE, McGrath EP, Cleary P, et al. Inhibition of IRE1 RNase activity modulates the tumor cell secretome and enhances response to chemotherapy. *Nat Commun*. 2018;9. doi:10.1038/s41467-018-05763-8
35. Seidel C, Oechsle K, Lorch A, et al. Efficacy and safety of gemcitabine, oxaliplatin, and paclitaxel in cisplatin-refractory germ cell cancer in routine care-Registry data from an outcomes research project of the German Testicular Cancer Study Group. *Urol Oncol Semin Ori*. 2016;34:120.
36. Yuan Y, Lee JS, Yost SE, et al. Phase II trial of neoadjuvant carboplatin and nab-paclitaxel in patients with triple-negative breast cancer. *Oncologist*. 2021;26:E382–E393. doi:10.1002/onco.13574
37. Abu Samaan TM, Samec M, Liskova A, Kubatka P, Busselberg D. Paclitaxel's mechanistic and clinical effects on breast cancer. *Biomolecules*. 2019;9:789. doi:10.3390/biom9120789
38. Della Corte L, Barra F, Foreste V, et al. Advances in paclitaxel combinations for treating cervical cancer. *Expert Opin Pharmaco*. 2020;21:663–677. doi:10.1080/14656566.2020.1724284
39. Futamura M, Oba M, Masuda N, et al. Meta-analysis of nanoparticle albumin-bound paclitaxel used as neoadjuvant chemotherapy for operable breast cancer based on individual patient data (JBCRG-S01 study). *Breast Cancer*. 2021;28:1023–1037. doi:10.1007/s12282-021-01238-9
40. Hyun H, Park MH, Jo G, et al. Injectable glycol chitosan hydrogel containing folic acid-functionalized cyclodextrin-paclitaxel complex for breast cancer therapy. *Nanomaterials-Basel*. 2021;11. doi:10.3390/nano11020317
41. Weaver BA, Bement W. How Taxol/paclitaxel kills cancer cells. *Mol Biol Cell*. 2014;25:2677–2681. doi:10.1091/mbc.e14-04-0916
42. Lee H, Park S, Kang JE, Lee HM, Kim SA, Rhie SJ. Efficacy and safety of nanoparticle-albumin-bound paclitaxel compared with solvent-based taxanes for metastatic breast cancer: a meta-analysis. *Sci Rep*. 2020;10:125.
43. Yu J, Mu QX, Perazzolo S, et al. Novel long-acting drug combination nanoparticles composed of gemcitabine and paclitaxel enhance localization of both drugs in metastatic breast cancer nodules. *Pharm Res*. 2020;37. doi:10.1007/s11095-020-02888-8
44. Zajdel A, Wilczok A, Jelonek K, et al. Cytotoxic effect of paclitaxel and lapatinib co-delivered in polylactide-co-poly(ethylene glycol) micelles on HER-2-negative breast cancer cells. *Pharmaceutics*. 2019;11:169. doi:10.3390/pharmaceutics11040169
45. Huang QX, Kuok KI, Zhang XJ, et al. Inhibition of drug-induced seizure development in both zebrafish and mouse models by a synthetic nanoreceptor. *Nanoscale*. 2018;10:10333–10336. doi:10.1039/C8NR02041H

46. Lee KJ, Nallathamby PD, Browning LM, Osgood CJ, Xu XHN. In vivo imaging of transport and biocompatibility of single silver nanoparticles in early development of zebrafish embryos. *Acs Nano*. 2007;1:133–143. doi:10.1021/nn700048y
47. Ng ANY, De jong-curtain TA, Mawdsley DJ, et al. Formation of the digestive system in zebrafish: III. Intestinal epithelium morphogenesis. *Dev Biol*. 2005;286:114–135. doi:10.1016/j.ydbio.2005.07.013
48. Ryu B, Kim CY, Oh H, et al. Development of an alternative zebrafish model for drug-induced intestinal toxicity. *J Appl Toxicol*. 2018;38:259–273. doi:10.1002/jat.3520
49. Chen TK, Liu W, Xiong S, et al. Nanoparticles mediating the sustained puerarin release facilitate improved brain delivery to treat Parkinson's disease. *Acs Appl Mater Inter*. 2019;11:45276–45289. doi:10.1021/acsami.9b16047
50. Rachmawati H, Pradana AT, Safitri D, Adnyana IK. Multiple functions of D-alpha-tocopherol polyethylene glycol 1000 succinate (TPGS) as curcumin nanoparticle stabilizer: in vivo kinetic profile and anti-ulcerative colitis analysis in animal model. *Pharmaceutics*. 2017;9:24. doi:10.3390/pharmaceutics9030024
51. Guo YY, Niu BN, Song QL, et al. RGD-decorated redox-responsive D-alpha-tocopherol polyethylene glycol succinate-poly(lactide) nanoparticles for targeted drug delivery. *J Mater Chem B*. 2016;4:2338–2350. doi:10.1039/C6TB00055J
52. Wu MJ, Huang T, Wang J, et al. Antilung cancer effect of ergosterol and cisplatin-loaded liposomes modified with cyclic arginine-glycine-aspartic acid and octa-arginine peptides. *Medicine*. 2018;97:112.
53. Hayati F, Chabib L, Fauzi IS, et al. Effects of pegagan (Centella asiatica L.) ethanolic extract SNEDDS (Self-nanoemulsifying Drug Delivery Systems) on the development of zebrafish (Danio rerio) embryos. *J Pharm Bioallied Sci*. 2020;12:457–461. doi:10.4103/JPBS.JPBS_297_19
54. Mo Y, Duan L, Yang Y, et al. Nanoparticles improved resveratrol brain delivery and its therapeutic efficacy against intracerebral hemorrhage. *Nanoscale*. 2021;13:3827–3840. doi:10.1039/D0NR06249A
55. Chen D, Zhang J, Tang Y, et al. A tumor-mitochondria dual targeted aza-BODIPY-based nanotheranostic agent for multimodal imaging-guided phototherapy. *J Mater Chem B*. 2018;6:4522–4530. doi:10.1039/C8TB01347K
56. Varela-Lopez A, Vera-Ramirez L, Giampieri F, et al. The central role of mitochondria in the relationship between dietary lipids and cancer progression. *Semin Cancer Biol*. 2021;73:86–100. doi:10.1016/j.semcancer.2021.01.001
57. Cannino G, Ciscato F, Masgras I, Sanchez-Martin C, Rasola A. Metabolic plasticity of tumor cell mitochondria. *Front Oncol*. 2018;8. doi:10.3389/fonc.2018.00333
58. Cardenas C, Lovy A, Silva-Pavez E, et al. Cancer cells with defective oxidative phosphorylation require endoplasmic reticulum-to-mitochondria Ca2+ transfer for survival. *Sci Signal*. 2020;13. doi:10.1126/scisignal.aay1212

International Journal of Nanomedicine Dovepress

Publish your work in this journal

The International Journal of Nanomedicine is an international, peer-reviewed journal focusing on the application of nanotechnology in diagnostics, therapeutics, and drug delivery systems throughout the biomedical field. This journal is indexed on PubMed Central, MedLine, CAS, SciSearch®, Current Contents®/Clinical Medicine, Journal Citation Reports/Science Edition, EMBase, Scopus and the Elsevier Bibliographic databases. The manuscript management system is completely online and includes a very quick and fair peer-review system, which is all easy to use. Visit http://www.dovepress.com/testimonials.php to read real quotes from published authors.

Submit your manuscript here: https://www.dovepress.com/international-journal-of-nanomedicine-journal